Journal of the Optical Society of Korea, Vol. 6, No. 3, September 2002, pp. 76-82

Photonic Band Gaps for Surface Plasmon Modes in Dielectric Gratings on a Flat Metal Surface

Jaewoong Yoon, Gwansu Lee, Seok Ho Song*, Cha-Hwan Oh, and Pill-Soo Kim

Microoptics NRL, Dept. of Physics, Hanyang University, Seoul 133-791, KOREA

(Received April 2, 2002)

For dielectric gratings on a flat metal surface, photonic band gaps created by Bragg scattering of surface plasmon polaritons are observed. The observation result that directly images this gap is compared with that predicted by a numerical model based on a plane wave expansion. Consistency between the experimental and numerical results is also confirmed by comparison with the well-known calculation method of diffraction, the rigorous coupled wave analysis method.

OCIS codes : 240.6680, 240.6690.

I. INTRODUCTION

In the propagation of electromagnetic modes, it is noted that surface modes are a useful system for examining some of the basic physics of photonic band gaps(PBG's) both in experiment and theory. [1,2] One of the reasons can be pointed out that surface modes require only a periodically modulated two-dimensional (2-D) structure to produce an energy gap, while bulk modes require 3-D periodic structures. Energy gaps produced in the propagation of surface modes, especially surface plasmon polaritons (SPP's) on metallic 2-D gratings, have been explained in an analytic model and reported in an experiment that directly image the gaps. [2,3] In their analytic modeling, the 2-D corrugated metal surface is flattened by making use of appropriate coordinate transformation, and the Maxwell equations are expressed in the new transformed coordinate system. Expressions of the gap width and the central frequency are derived for the case when first order Bragg scattering is only considered.

In order to fully understand many physical phenomena related on PBG's, however, corrugated metallic surfaces may not be enough to represent a general case of PBG structures, since most of the PBG materials used in a number of applications proposed so far are dielectric. We report in this paper on surface plasmon band gaps that arise for the propagation of SPP's through dielectric gratings on a flat metallic surface. In Section 2 we discuss a brief background on different concept between the two cases of the metallic gratings and the dielectric gratings. In Sec. 3, we present a wide band gap of SPP's observed by direct imaging technique used previously [3], which arises from periodic media of the dielectric gratings even with a grating depth of few tens of nanometers. Such a wide band gap is obtained from very shallow periodic structure mainly due to the large field enhancement property of the SPP. The field enhancement is about 10 $\sim$ 100 times larger than evanescent waves for SPP resonance. In Sec. 4, a full numerical model based on a plane wave expansion is also developed to predict the surface plasmon energy gaps of dielectric gratings. Actually, the energy band gaps of a dielectric lattice consisting of two different dielectric materials are of the results from different mode frequencies at a given wavevector. The different modes can be obtained by interference between diffraction modes of Bragg scattered fields. Therefore, we are able to confirm a consistency between the experimental and numerical results by comparison with the well-known calculation method of diffraction, the rigorous coupled wave analysis method. Finally, we will summarize our results in Sec. 5.

II. BACKGROUND

The SPP's are nonradiative TM polarized modes of collective oscillation of free charged particles which are propagating along the metal/dielectric interface. Because the SPP's have wavevectors larger than those of photons with the same energy, one way to excite the

SPP's is to use an attenuated total reflection (ATR) configuration. A typical ATR device consists of a dielectric high-index prism and a thin metal film on a prism surface. The metal film is regarded as a tank of free electron gas from a macroscopic point of view, and it is sufficiently thin to allow most of the incident optical energy to penetrate through it. Above the critical angle of internal reflection, both of the TM- and TE-polarization components of the incident light beam are totally reflected from the prism-metal interface. At a certain angle after the total reflection, on the other hand, only the incident TM-component is completely absorbed to the interface, and then a surface mode of the SPP is generated with the help of the momentum-matching condition, or surface plasmon resonance (SPR) condition. The wave number, k_{sp} , at SPR is given by [4].

$$k_x = \frac{\omega}{c}\sqrt{\varepsilon_p}\sin\theta = k_{sp} = \frac{\omega}{c}\left(\frac{\varepsilon_m \varepsilon_g}{\varepsilon_m + \varepsilon_g}\right)^{1/2} \qquad (1)$$

It means that the component of the incident wave vector in the plane parallel to the metal layer, k_x , is exactly matched to the propagation vector of the surface plasmon, k_{sp} . In the Eq. (1), ε_p , ε_m , and ε_g are dielectric constants of the prism, the metal, and the dielectric material above the metal film. At the SPR condition, the surface mode reaches its maximum field which is confined within the wavelength height in the normal direction from the interface between the metal and the dielectric. The confined surface field as a nonradiative TM polarized mode of collective oscillations of free charged particles then propagates through the interface. Therefore the field intensity is dramatically enhanced about $10 \sim 100$ times larger than another surface mode of evanescent fields generated from an interface between two dielectric media. This large field enhancement characteristic of the SPP's has been applied to implementation of many optical devices, such as light modulators [5]- [9], optical switching [10], optical filters [11]- [14], polarization beam splitters [15] and second harmonic generators [16].

One of the interesting studies to understand interaction of SPP's with periodic media is of surface plasmon band gaps. It has been reported that SPP's excited on a periodically corrugated metallic surface reveal energy band gaps that prohibit the propagation of modes over a range of optical frequencies [1,4]. Inhibiting excitation of surface modes by opening complete band gaps [1], coupling SPP's to radiation fields [17], and channel guiding of SPP's [18] had been reported. Especially Barnes et al's works showed full surface plasmon band gaps in the visible from periodically corrugated metal surfaces [1] and proposed an analytic model for the width and the central frequency of surface plasmon band gaps [2]. In their analytic modeling, a corrugated surface of metal gratings is flattened by making use of appropriate coordinate transformation, and then Maxwell equations are expressed in the new coordinate system. Solutions for the surface modes that propagate on the metal gratings are based on the first order Bragg scattering with boundary conditions at the metal-air interface. The analytic expressions for the mode frequencies at band gap edges are of the form,

$$\left(\frac{\omega_\pm}{c}\right)^2 = \left(\frac{\omega_0}{c}\right)^2 (1 - 2(Kd)^2) \pm 2(Kd)\frac{K^2}{\sqrt{-\varepsilon_M \varepsilon_D}}(1 - 3(Kd)^2) \qquad (2)$$

where ω_0, K, d and are the mode frequency for no corrugation in the metal, the magnitude of the primitive reciprocal lattice vector, and the depth of the metallic corrugation, respectively. They showed that the physical origin of the surface plasmon band gap would be found from the fact that two standing wave solutions of SPP modes take different positions with respect to the peaks and troughs of the grating. It means that the electromagnetic field and surface charge distributions of a nonradiative SPP mode will differ in the two modes. We can say that there is a difference in penetration depth (or, decay length) of the electromagnetic field into the surrounding dielectric media between the two modes; one coupled out from the surface charge distribution which has most of its charge density on the peaks of the corrugation and the other which has most of its charge density on the troughs of the corrugation. The former mode has the lower frequency solution at the surface plasmon energy band gap and the latter has the higher frequency solution.

In this paper, on the other hand, we present another system to exhibit surface plasmon band gaps. Our system consists of a dielectric grating layer on a flat metal surface, instead of the corrugated metallic gratings. Thus, the physical origin of the energy band gaps in our system may differ from that in the metallic grating system. As a 1-D PBG structure, consider a dielectric grating consisting of two different dielectric media with a period of a. If the condition that $k_{SD} = \pi/a$ is satisfied there will be two standing surface modes in the dielectric media. The two modes result from Bragg reflection of the electromagnetic field in the nonradiative SPP wave, and they have different energies. This difference arises because the electromagnetic fields of the two modes are concentrated in regions of different optical permittivity.

III. EXPERIMENTAL RESULTS

We have measured a dispersion curve of the SPP's and a surface plasmon band gap by the direct imaging technique [3]. As shown in Fig. 1, the imagingl set-up

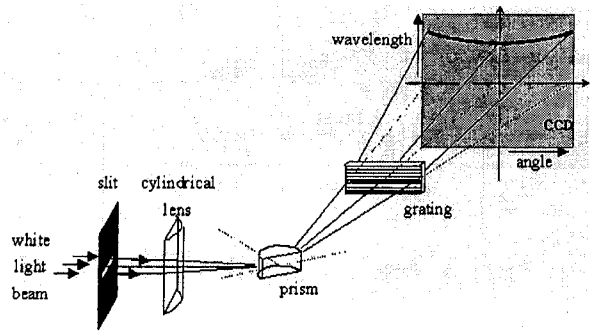

FIG. 1. A schematic of the experimental set-up.

is similar to the arrangement of Ref. 3, except a transmission grating is used instead of a reflection grating to split the energies in one direction. A TM-polarized and collimated white light is made incident on a horizontal slit. The light is then focused through a cylindrical lens on a thin (52nm) silver film deposited onto the base of a hemi-cylindrical prism. This light contains photons of a range of energies and momenta. Specific photons whose energies and momenta match the SPP's will be absorbed on the silver-air interface, and the rest of the photons will be reflected from the interface. A transmission grating is used to spread out the reflected photons in the vertical direction, which corresponds to wavelength spectra. Photographs of the SPP's dispersion curves are therefore obtained from a color CCD camera.

First we have measured a typical dispersion relation of the SPP's by using the imagine set-up. Fig. 2 is a photograph of the dispersion curve of SPP's which propagate on the flat silver surface. The dark arc in the photograph shows us clearly a dispersion relation of the SPP's. The horizontal axis represents the incidence angles (momenta) of the white light and the vertical axis is related to the wavelength (energy) of the light. The A and B points marked on the vertical axis represent the wavelengths of 633nm and 460nm for calibration. We used two narrow (2nm) band-pass filters for the calibration, and they will give us important landmarks to measure central frequencies and widths of the surface plasmon band gaps in later on.

As one of the dielectric PBG structures, now consider a 1-D grating layer constructed on the flat surface of the thin silver film. Fig. 3(a) shows a clear energy gap near the top of the reddish region. In this band gap measurement, we have used a photoresist holographic linear grating, with a period of 256nm and a modulation depth of 80nm. The boxes shown in Fig. 3(b) reveal the dispersion relations calculated by the rigorous coupled wave analysis (RCWA). By comparing the photograph with the calculated curves, we are able to find the width of the surface plasmon band gap ($\Delta\omega = \omega_+ - \omega_-$) to be 0.016 times the plasma frequency ($\omega_D = 1.274 \times 10^{16}/s$) of the silver film. We will not go further here in detail about the calculation process of the RCWA since one can find many references on the RCWA in other places [20]. However, physics related to the SPP's band gap for the dielectric PBG structure will be discussed further in Sec. 4, where a more intuitive numerical model to calculate the SPP's band gaps is introduced.

It should be noted that in Fig. 3 the dispersion curves showing the band gap have a slope much flatter than the slope shown in Fig. 2. Lowering cut-off frequency of the SPP as the effective dielectric constant of the dielectric layer increases makes the slop of flatter. If there is no dielectric grating layer on the silver film surface, the cut-off frequency would be $\omega_D/\sqrt{2}$. But, with the dielectric layer which has an effective dielectric constant, ε_d which is larger than one, the cut-off frequency is reduced to be $\omega_D/\sqrt{1+\varepsilon_d}$. We can also approximately imagine the origin of the energy gap before doing a rigorous calculation as follow. Mode frequency of SPP's is given by [4]

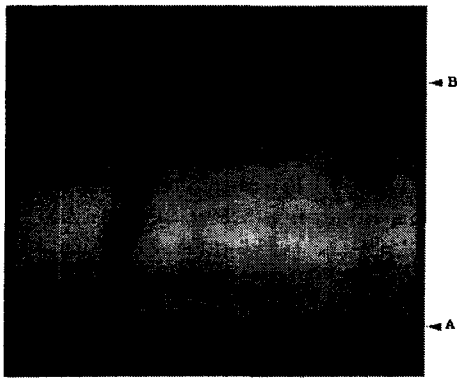

FIG. 2. A photograph showing the dispersion curve of SPP's for silver and air interface.

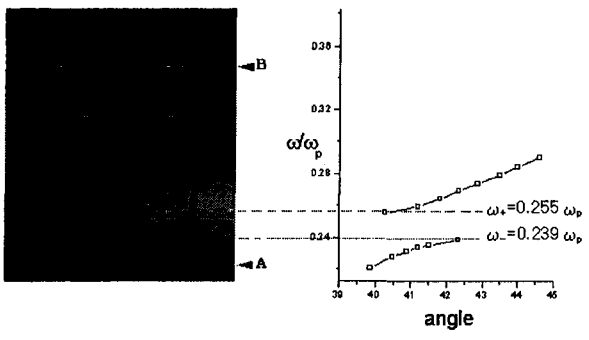

FIG. 3. (a) A photograph of the SPP's band structure and (b) the RCWA result when $\omega_p = 1.274 \times 10^{16}$Hz).

$$\omega(k_{sp}) = \frac{\omega_p}{\sqrt{2}}\left[1+(1+\frac{1}{\varepsilon_d})\left(\frac{ck_{sp}}{\omega_p}\right)^2 - \sqrt{\left\{1+(1+\frac{1}{\varepsilon_d})\left(\frac{ck_{sp}}{\omega_p}\right)^2\right\}^2 + \frac{4}{\varepsilon_d}\left(\frac{ck_{sp}}{\omega_p}\right)^2}\right]^{1/2} \quad (3)$$

where k_{sp} is the wave number defined in Eq. (1). Assume that ε_1 and ε_2 are the dielectric constants of the two alternative dielectric media in the grating layer with a period of a. There will be two different standing waves in the dielectric media, which are generated by interference between the SPP's suffering from Bragg reflection. Most of the electromagnetic field distribution may be concentrated into either one of the two dielectric media for the respective one of the standing waves. Therefore, there will be two different mode frequencies of ω_1 and ω_2 which can be determined from the Eq. (3) for the cases when $\varepsilon_d = \varepsilon_1$ and $\varepsilon_d = \varepsilon_2$, respectively. The difference in the mode frequencies implies, in consequence, a reason why the energy gap of SPP's occurs in dielectric PBG structures on a flat metal surface.

IV. SPP'S BAND GAP CALCULATION BASED ON PLANE WAVE EXPANSION METHOD

1. Numerical modeling by use of the plane wave expansion method

A numerical model we develop here is mainly based on the plane wave expansion method (PWEM), which is widely used in the band gap calculation of dielectric PBG structures [19,21]. The reason why we are able to use the same method to calculate the band gaps of SPP's is that a nonradiative SPP mode consists of an evanescent electromagnetic field oscillation coupled to an oscillating surface charge distribution. In our case for the propagation of SPP's through dielectric gratings on a flat metallic surface, the evanescent electromagnetic field propagates on the flat metallic surface with a strong perturbation from the dielectric grating structures. To calculate surface plasmon band gaps is, therefore, the same work as to do band gaps for the evanescent field by expanding it into many plane wave components.

The problem to calculate band structures of SPP's may start with an eigenvalue problem induced from the two curl expressions of the Maxwell equations,

$$\nabla \times \frac{1}{\varepsilon(\vec{x})}\nabla \times \vec{h_\omega}(\vec{x}) = \left(\frac{\omega}{c}\right)^2 \vec{h_\omega}(\vec{x}), \quad (4)$$

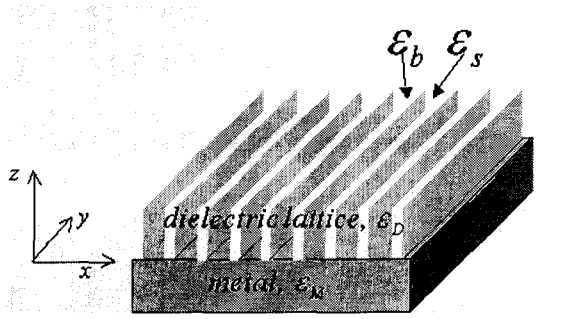

FIG. 4. A system for band structure calculation. Thickness of the metal and the dielectric lattice is assumed to be semi-infinite in the numerical model.

$$\vec{H_\omega}(\vec{x},t) = Re\{\vec{h_\omega}(\vec{x})e^{-i\omega t}\}, \quad (5)$$

where $\vec{H_\omega}$ is the magnetic field of a monochromatic EM wave with the frequency of $\omega$and its complex amplitude function of $\vec{h_\omega}$. $\varepsilon(\vec{x})$ is a dielectric function of the dielectric layer. Choosing the magnetic field for wave equations makes the problem simple since the electric field is not Hermitian in the dielectric lattice structure [19]. Now consider an optical system consisting of a dielectric lattice in the region of $z > 0$ and a flat metal in $z < 0$ as shown in Fig. 4. It is assumed that the metal and the dielectric have semi-infinite thickness. The dielectric function can be represented in the form of

$$\varepsilon(\vec{x}) = \left\{ \begin{array}{ll} \varepsilon_D(\vec{x}) & (z>0) \\ \varepsilon_M & (z<0) \end{array} \right\}, \quad (6)$$

where, $\varepsilon_D(\vec{x}) = \varepsilon_s + \sum_n(\varepsilon_b - \varepsilon_s)Basis(\vec{x} - \vec{R_n})$, $Basis(\vec{x}) = \left\{ \begin{array}{ll} 1 & \text{(in the basis)} \\ 0 & \text{(in the substrate)} \end{array} \right\}$, the lattice translation vector of $\vec{R_n} = l_{n1}\vec{a_1} + l_{n2}\vec{a_2}$ $\left(\begin{array}{l} l_{n1}, l_{n2} : \text{integer} \\ \vec{a_1}, \vec{a_2} : \text{primitive lattice vector} \end{array} \right)$, and $\varepsilon_M = 1 - \frac{\omega_p^2}{\omega^2}$ (ω_p : plasma frequency of the metal). The periodic ε_D in Eq. (6) can be further expanded with harmonics of plane waves whose wavevectors are reciprocal lattice vectors given by $\vec{G_n} = \nu_{n1}\vec{b_1} + \nu_{n2}\vec{b_2}$ (ν_{n1}, ν_{n2} : integer),

$$\varepsilon_D(\vec{x}) = \sum_n \tilde{\varepsilon}(\vec{G_n})e^{i\vec{G_n}\cdot\vec{x}}, \quad \tilde{\varepsilon}(\vec{G_n}) = \frac{1}{S_{\text{unit cell}}}\int_{\text{unit cell}} dx\,dy\varepsilon_D(\vec{x})e^{-i\vec{G_n}\cdot\vec{x}} \quad (7)$$

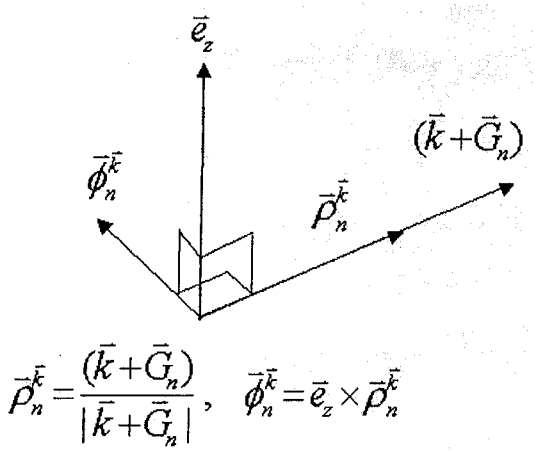

FIG. 5. Relation between polarization unit vector,$\vec{\phi}_n^{\vec{k}}$, and wavevector of nth plane wave component,$\vec{\rho}_n^{\vec{k}}$.

The primitive reciprocal lattice vectors are defined by $\vec{b_1} = 2\pi\frac{\vec{a_2}\times\vec{z}}{\vec{a_1}\times\vec{a_2}\cdot\vec{z}}$ and $\vec{b_2} = 2\pi\frac{\vec{z}\times\vec{a_1}}{\vec{a_1}\times\vec{a_2}\cdot\vec{z}}$. The calculation process to solve the eigenvalue problems of Eq. (3) can be completed by the following procedures: Expanding the complex amplitude function, $\vec{h_\omega}$, with a set of plane waves, $\{e^{i\vec{G_n}\cdot\vec{x}}\}$; solving the Eq. (4) for the metal region with ε_M; solving the Eq. (4) for the dielectric lattice region with ε_D in Eq. (7); applying boundary conditions at the interface between the metal and dielectric; finally solving coupled matrix equations. We assume that the complex amplitude function is a Bloch-Floquet mode, because the system has a discrete translational symmetry along in $x-y$ plane, and that $\nabla\cdot\vec{h_\omega} = 0$, because there are no magnetic materials. The for a TM-polarized evanescent field is expressed as

$$\vec{h}_{\omega,\vec{k}}(\vec{x}) = [\sum_n h_n^{\omega,\vec{x}}(z)\vec{\phi}_n^{\vec{k}}e^{i\vec{G_n}\cdot\vec{x}}]e^{i\vec{k}\cdot\vec{x}} \tag{8}$$

where $\vec{e_z}$ and $\vec{\phi}_n^{\vec{k}}$ are unit vectors of the z-axis and the polarization direction as shown in Fig. 5, and $\vec{k}$ a Bloch wavevector which is placed in $x-y$ plane. Now, the problem is to decide the amplitudes of the plane waves $h_n^{\omega,\vec{k}}(z)$ and the eigenvalue ω/c. In the metal region, Eq. (4) gives us the solutions of

$$\vec{h}_{\omega,\vec{k}}(x,y;z<0) = [\sum_n h_n^{\omega,\vec{k}}(0)e^{-k_n z}e^{i\alpha_n z}\vec{\phi}_n^{\vec{k}}]e^{i(\vec{k}+\vec{G_n})\cdot\vec{x}}, \tag{9}$$

where

$$\left\{\begin{array}{l}\kappa_n = \left[\frac{1}{2}\left\{A^2(\vec{k},\omega,n)+\sqrt{A^4(\vec{k},\omega,n)+B^4(\omega)}\right\}\right]^{1/2} \\ \alpha_n = \dfrac{B^2(\omega)}{\left[2\left\{A^2(\vec{k},\omega,n)+\sqrt{A^4(\vec{k},\omega,n)+B^4(\omega)}\right\}\right]^{1/2}}\end{array}\right\}$$

and $\left\{\begin{array}{l}A^2(\vec{k},\omega,n) = |\vec{k}+\vec{G_n}|^2-\varepsilon_r k_0^2 \\ B^2(\omega) = \varepsilon_i k_0^2\end{array}\right\}$.

In the dielectric lattice region, Eq. (4) does not give us an explicit solution since the plane waves are coupled to each other. But it can be expressed in matrix form as follows;

$$\sum_m \tilde{\eta}_{nm}[|\vec{k}+\vec{G_n}||\vec{k}+\vec{G_m}|h_m^{\omega,\vec{k}}(z) - \cos\phi_{nm}^{\vec{k}}\frac{d^2}{dz^2}h_m^{\omega,\vec{k}}(z)] = \left(\frac{\omega}{c}\right)^2 h_n^{\omega,\vec{k}}(z) \tag{10}$$

where $\tilde{\eta}_{nm}$ is Fourier transform of the $1/\varepsilon(\vec{x})$ with the spatial frequency of $\vec{G_n}-\vec{G_m}$, and $\phi_{nm}^{\vec{k}}$ is the angle between $\vec{\phi}_n^{\vec{k}}$ and $\vec{\phi}_m^{\vec{k}}$. Each of the solutions for $\vec{h}_{\omega,\vec{k}}(\vec{x})$ in the metal, Eq. (9), and the dielectric lattice, Eq. (10), must satisfy two boundary conditions given from the Maxwell equations as follows;

$$[h_n^{\omega,\vec{k}}(0)]_{\text{metal}} = [h_n^{\omega,\vec{k}}(0)]_{\text{dielectric}}, \tag{11}$$

$$\frac{1}{\varepsilon_m}[\frac{d}{dz}h_n^{\vec{k},\omega}(0)]_{\text{metal}} = \sum_m \tilde{\eta}_{nm}\cos\phi_{nm}^{\vec{k}}[\frac{d}{dz}h_m^{\vec{k},\omega}(0)]_{\text{dielectric}}. \tag{12}$$

Finally, we can obtain two coupled matrix equations by applying boundary conditions of Eqs. (11) and (12) to Eqs. (9) and (10),

$$\sum_m \tilde{\eta}_{nm}\cos\phi_{nm}^{\vec{k}}\beta_m h_m^{\omega,\vec{k}}(0) = \frac{\alpha_n+i\kappa_n}{\varepsilon_M}h_n^{\omega,\vec{k}}(0), \tag{13}$$

$$\sum_m L_{nm}^{\omega,\vec{k}}h_m^{\omega,\vec{k}}(0) = \left(\frac{\omega}{c}\right)^2 h_n^{\omega,\vec{k}}(0), \tag{14}$$

where, $L_{nm}^{\omega,\vec{k}} = \tilde{\eta}_{nm}[|\vec{k}+\vec{G_n}||\vec{k}+\vec{G_m}| - \cos\phi_{nm}^{\vec{k}}\beta_m^2]$. At a fixed frequency, from the Eq. (13) we first determine the values of $\{\beta_n\}$ which are independent on $\{h_n^{\omega,\vec{k}}(0)\}$, and then we find the values of $\vec{k}$ in the first Brillouin zone by solving the Eq. (14). Finally, the dispersion relation between momentum of $\vec{k}$ and frequency of ω for SPP's can be obtained.

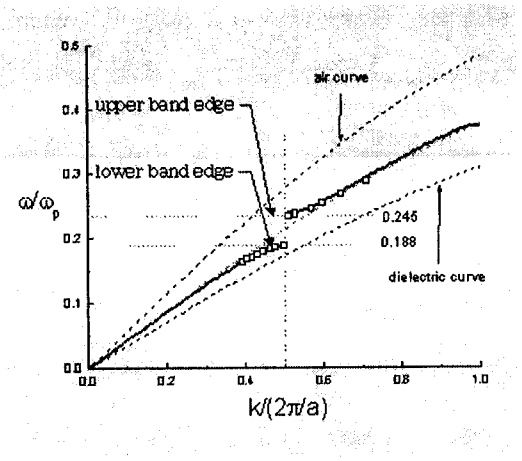

FIG. 6. SPP's band structures obtained by PWM(−) and RCWA(□), when $a = 1.5\lambda_p$.

2. Comparison of the SPP's band structures calculated by PWEM with RCWA

In fact, the PWEM-based numerical model described above assumed that the metal and the dielectric grating have semi-infinite thickness as shown in Eq. (6). However, the property that the SPP's propagate only on the interface between the metal and dielectric makes it possible to estimate intuitively characteristics of the SPP's band structure without loss of generality. Therefore, by keeping the assumption of the semi-infinite thickness, we will compare two band structures obtained from the PWEM-based model and the RCWA in accordance with Fig. 6, and will discuss the dependence of the central frequency and width of the SPP's band gaps on lattice constant in Fig. 7.

In Fig. 6, a SPP's band structure (solid curves) calculated by the PWEM-based model is presented. The horizontal axis is normalized by $2\pi/a$, but the vertical axis of frequency by ω_p. The boxes between two dispersion relations (dashed lines) of the air curve and the dielectric curve represent the results calculated by the RCWA near the energy band gap. In the calculation, we assumed that a 1-D dielectric grating consists of air and dielectric material ($\varepsilon_D = 2.56$). The silver metal film having the plasma frequency of $\omega_p = 1.274 \times 10^{16}$ Hz is used again. The dielectric filling ratio is 0.5 and the lattice constant, a, is 256 nm ($a = 1.5\lambda_p$, where $\lambda_p = 2\pi c/\omega_p$). Both the results showing a SPP band gap ranging from the lower band edge of $0.188\omega_p$ to the upper band edge of $0.245\omega_p$ are very consistent with each other. The SPP band gap in this case corresponds to a wavelength range from 600 nm to 783 nm. It is noted that the lower band edge shifts more closely to the dielectric curve than the shift of the upper band edge to the air curve. This implies the origin of the SPP band gap in a dielectric lattice: The mode of a standing wave at the lower (upper) band edge has its most field concentrated into the dielectric (air) region, and TM-polarized EM waves of the SPP's prefer penetrating into the dielectric region.

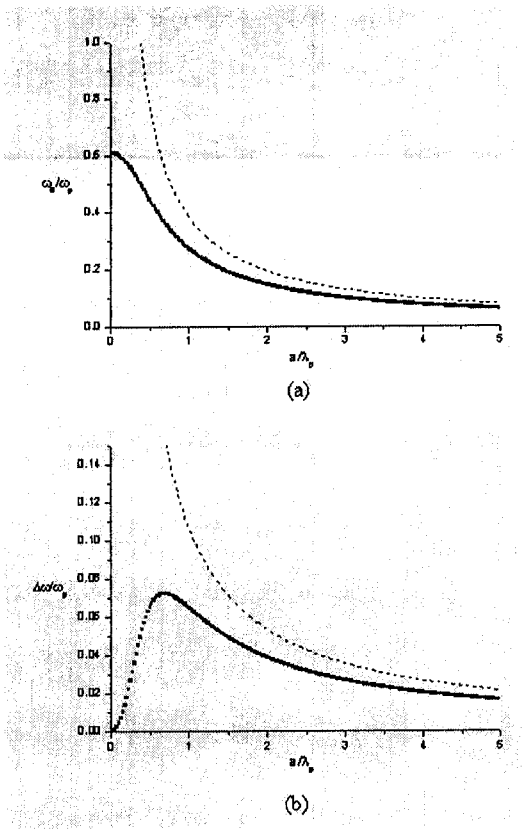

FIG. 7. Dependence of the central frequency in (a) and the width in (b) of the SPP's on lattice constant, a.

Fig. 7 shows dependence of the SPP's band structure on the lattice constant. Variation of the normalized central frequency, ω_0/ω_p, with the normalized lattice constant, a/λ_p, is shown in Fig. 7(a). The dashed curve in this figure is of a bulk light-wave propagating on the semi-infinite dielectric lattice. When the lattice constant a becomes smaller, the central frequency of the SPP's approaches its maximum value of the cut-off frequency, $\omega_p/\sqrt{2}$, while that of the bulk wave diverges to infinite. The band gap width of the SPP's shown in Fig. 7(b) has also its maximum when $a = 0.7\lambda_p$ without diverging like that of the bulk wave. It is found that, therefore, the SPP band structure is no more than scalable in the lattice constant. The cut-off frequency inhibits increase of the SPP's both in the central frequency and the width. These properties of the SPP's band structure are coincident with the results of Ref. 22.

V. CONCLUSION

We have observed experimentally the photonic band gap in dispersion curves of SPPs excited at a 1-D dielectric lattice structure on a flat metal surface. Even though modulation depth and refractive index of the dielectric lattice are very small, a clear and wide band structure has been measured by a direct imaging technique. The result of direct imaging has been completely overlapped with the calculation result of the RCWA. We have also presented a numerical method based on plane wave expansion in order to understand intuitively the properties of the SPP's band structures, such as dependence of the central frequency and the width of the SPP's band gap on lattice constant. We have found that the photonic band structure of SPP's is no more than scalable in the lattice constant, which would be quite different from the scalability of photonic band structures for bulk light-waves. It is expected that there are many interesting subjects related to interaction between SPP's and dielectric lattices. Some of them are designing SPP dispersion by use of dielectric lattice at a fixed frequency range, analyzing effects of large enhancement of density of state at a band edge, obtaining complete SPP band gaps from 2-D dielectric lattices, enhancing nonlinear effect on SPR, applying SPP resonance on magnetic materials, coupling SPP fields to radiation fields, and so on. They are future works of our SPP related research.

ACKNOWLEDGEMENT

This work was supported by the 1999 grant of Hanyang University.

*Corresponding author : shsong@hanyang.ac.kr.

REFERENCES

[1] S. C. Kitson, W. L. Barnes, and J. R. Sambles, Phys. Rev. Lett. **77**, 2670 (1996).
[2] W. L. Barnes, J. D. Preist, and J. R. Sambles, Phys. Rev. B **54**, 6227 (1996).
[3] S. C. Kitson, W. L. Barnes, G. W. Bradberry, and J. R. Sambles, J. Appl. Phys. **79**, 7383 (1996).
[4] H. Reather, *Surface plasmons on smooth and rough surfaces and on gratings* (Springer-Verlag, 1988) chepter1.
[5] M. E. Caldwell and E. M. Yeatman, Appl. Opt. **31**, 3880 (1992).
[6] T. Okamoto, T. Kamiyama, and I. Yamaguchi, Opt. Lett. **18**, 1570 (1993).
[7] A. Yacoubian and T. M. Aye, Appl. Opt. **32**, 3073 (1993).
[8] B. Jung, S. Lee, and K. Kuhn, Appl. Opt. **34**, 946 (1995).
[9] M. Rosenbluh, and V. Sandomirsky, Appl. Phys. Lett. **68**, 882 (1996).
[10] K. Sasaki and T. Nagamura, Appl. Phys. Lett. **71**, 434 (1997).
[11] Y. Wang, Appl. Phys. Lett. **67**, 2759 (1995).
[12] P. J. Kajenski, Opt. Eng. **36**, 263 (1997).
[13] P. J. Kajenski, Opt. Eng. **36**, 1537 (1997).
[14] J. Homola, R. Slavik, and J. Ctyroky, Opt. Lett. **22**, 1403 (1997).
[15] S. Park, *Grating-assisted emission of surface plasma wave* (PhD Thesis, Hanyang Univ., 2000).
[16] H. J. Simon, D. E. Mitchell, J. G. Watson, Phys. Rev. Lett. **33**, 1531 (1974).
[17] P. T. Worthing, W. L. Barnes, Appl. Phys. Lett. **79**, 3035 (2001).
[18] S. I. Bozhevolnyi, J. Erland, K. Leosson, P. M. W. Skovogaard, and J. M. Hvam, Phys. Rev. Lett. **86**, 3008 (2001).
[19] J. D. Joannopoulos, R. D. Meade, and N. J. Winn, *Photonic Crystals: Modeling the flow of light* (Princeton Univ. Press, 1995) chepter 2.
[20] M. G. Moharam and T. K. Gaylord, J. Opt. Soc. Am. **72**, 1385 (1982).
[21] A. A. Maradudin, V. Kuzmiak, and A. R. McGurn, *Photonic band structures of systems with components characterized by frequency dependent dielectric functions* (Kluwer Academic Publisher, Photonic Band Gap Materials, 1996) pp. 271-318.
[22] V. M. Agranovich and D. L. Mills, *Surface Polaritons* (North-Holland Publishing Company, 1982).